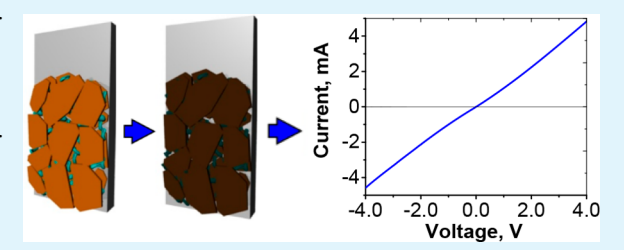
Cite This: ACS Appl. Mater. Interfaces 2018, 10, 3975–3985

Highly Conductive and Transparent Reduced Graphene Oxide Nanoscale Films via Thermal Conversion of Polymer-Encapsulated **Graphene Oxide Sheets**

Mykhailo Savchak,[†] Nikolay Borodinov,[†] Ruslan Burtovyy,[†] Mark Anayee,[†] Kesong Hu,^{||} Ruilong Ma,^{||} Anise Grant,^{||} Hongmei Li,[‡] Daniel B. Cutshall,[‡] Yimei Wen,[§] Goutam Koley,[‡] William R. Harrell,[‡] George Chumanov, Vladimir Tsukruk, and Igor Luzinov*, to

Supporting Information

ABSTRACT: Despite noteworthy progress in the fabrication of large-area graphene sheetlike nanomaterials, the vapor-based processing still requires sophisticated equipment and a multistage handling of the material. An alternative approach to manufacturing functional graphene-based films includes the employment of graphene oxide (GO) micrometer-scale sheets as precursors. However, search for a scalable manufacturing technique for the production of high-quality GO nanoscale films with high uniformity and high electrical conductivity is still continuing. Here we show that



conventional dip-coating technique can offer fabrication of high quality mono- and bilayered films made of GO sheets. The method is based on our recent discovery that encapsulating individual GO sheets in a nanometer thick molecular brush copolymer layer allows for the nearly perfect formation of the GO layers via dip coating from water. By thermal reduction the bilayers (cemented by a carbon-forming polymer linker) are converted into highly conductive and transparent reduced GO films with a high conductivity up to 10⁴ S/cm and optical transparency on the level of 90%. The value is the highest electrical conductivity reported for thermally reduced nanoscale GO films and is close to the conductivity of indium tin oxide currently in use for transparent electronic devices, thus making these layers intriguing candidates for replacement of ITO films.

KEYWORDS: graphene, graphene oxide film, nanoscale, transparency, conductivity

■ INTRODUCTION

There are a number of operative ways for obtaining mono- and multilayered graphene sheets, including epitaxial growth on SiC, chemical vapor deposition (CVD) on transition metals, solvothermal synthesis, mechanical exfoliation, and unzipping carbon tubes.¹⁻³ The predominant technique for obtaining larger-scale graphene film is CVD, which allows good control over synthesis, film thickness, and properties. The film, however, has to be transferred to a targeted substrate via a quite-sophisticated methodology for further device integration. For this reason, there is limited opportunity for scalability, with only two reports describing successful attempts to fabricate larger (10th of centimeter/meter) scale CVD-obtained graphene films via roll-to-roll transfer with low sheet resistance (150-500 Ω /sq without chemical doping) and high conductivity (10⁴ S/cm).^{4,5} We note that the transferred films had a significant density of defects (e.g., cracks, wrinkles, multilayered islands, nonuniformity, and impurities), especially for the monolayer and bilayered graphene films. Another film formation strategy uses the dispersion of graphene flakes obtained by various techniques and their deposition on solid

substrates. However, during the assembly of these flakes into larger area films/coatings with a thickness on the order of several nanometers via spin-coating, spraying, printing, dipcoating, the Langmuir-Blodgett [L-B] method, layer-by-layer [L-b-L] deposition, and drop-casting, the electrical characteristics of the films are significantly reduced in comparison to individual graphene sheets mostly due to imperfect film morphology and high sheet-to-sheet contact resistivity.² In fact, for these films a conductivity of $10^2 - 10^3$ S/cm and sheet resistance on the level of $10^3 \Omega/\text{sq}$ and higher are usually reported, 1,2,6-10 which are significantly lower than those known for widely exploited transparent conductive ITO film ($\sim 10^4$ S/ cm^{11,12}).

At this level of performance for the conductive films prepared from graphene flakes an alternative approach to building ultrathin and transparent highly conductive graphene-based layers with the employment of GO micrometer-scale flakes has

Received: October 30, 2017 Accepted: December 29, 2017 Published: December 29, 2017

[†]Department of Materials Science and Engineering, ‡Department of Electrical and Computer Engineering, and §Department of Chemistry, Clemson University, Clemson, South Carolina 29634, United States

School of Materials Science and Engineering, Georgia Institute of Technology, Atlanta, Georgia 30332, United States

appeared to be a strong contender.^{2,13} GO sheets serve as a "precursor" for its electrically conductive derivative, so-called reduced graphene oxide (rGO).¹ The approach has significant potential to rapidly grow to industrial scale. In fact, GO possesses several advantages over pristine graphene materials from a manufacturing point of view: it is inexpensive and can be produced at a large scale from readily available graphite.¹⁴ In addition, GO has excellent dispersibility in polar solvents, including water,¹⁵ and its surface can be straightforwardly modified.¹⁶ Therefore, GO has extreme adaptability and compatibility with various liquid media and solid substrates, which are important for the employment of standard methods of layer nanomanufacturing.^{17,18} In fact, significant progress has been reached in this area over the past decade, as described in a number of comprehensive review articles on the topic.^{1,2,7,13,19,20}

In wet-fabrication approaches, GO nanoscale layers have been assembled using spin-coating, spraying, dip-coating, L-B, L-b-L, electrophoretic, interfacial self-assembly, and drop-casting methods. 1,2,7,13,19,20 Among the methods used for the formation of rGO layers dip-coating, spray-coating, and dropcasting have the highest potential to be used for the manufacturing of larger scale conductive and transparent coatings. However, to the best of our knowledge there are no reports in the scientific literature describing the formation of highly conductive rGO nanoscale layers with a well-defined morphology and properties by these methods. As of today, the most-used method for obtaining several-nanometers-thick rGO films is spin-coating, which, indeed, allowed the production of highly conductive nanoscale rGO films. 1,2,21-23 The best results for the rGO films in terms of perfectness of morphology and electrical/optical properties were also obtained using L-B deposition^{24–26} and interfacial self-assembly.²⁷ The best fewnanometers-thick rGO films have a conductivity reported by authors to be 2×10^3 S/cm²¹ and sheet resistance to be on the level of 500–1100 Ω /sq.^{21,24–27} In terms of optical transparency, rGO demonstrates promising results as well, where the transparency reported for the highly conductive films is between 85% and 91%. ^{21,24–27} Using the direct current to optical conductivity ratio $(\sigma_{\rm DC}/\sigma_{\rm OP})$ as a figure of merit (Supporting Information, eq S1), the rGO films with a ratio of 2-7 are on the same level as graphene films grown by CVD on Ni $(\sigma_{DC}/\sigma_{OP} = 2-6)$ and Cu $(\sigma_{DC}/\sigma_{OP} = 10-12)$ substrates. 26,2

There are at least two major challenges for the layers made of rGO sheets: (i) the properties/morphology of individual rGO sheets and (ii) the properties/morphology of the rGO layers. At the individual rGO sheet level, one has to deal with only a partial reduction of the original GO,²⁸ the presence of numerous defects,²⁹ and a mosaic of conductive and nonconductive parts.³⁰ All these features reduce the material's ability to conduct electric current. In addition, at the GO layer level, the availability of GO (rGO) only in the form of micrometer size sheets causes high intersheet contact resistivity. This resistivity originates from untight/imperfect sheet arrangements/contacts in plane (edge-to-edge) and plane-to-plane (stacking) contacts. Therefore, striving for a thinner rGO layer to achieve the largest transparency value dramatically decreases the overall electrical—optical property balance with increase of the contribution of the intersheet resistivity, thus suppressing the facile formation of highly conductive and transparent flexible films for prospective micro/nanoelectronic applications.

To this end, this work reports on nanomanufacturing by the dip-coating and thermal reduction of the highly conductive rGO-based nanoscale layers possessing suppressed intersheet resistivity surpassing anything reported to date. The method is based on our recent discovery that (a) encapsulating individual GO sheets in a nanometer thick copolymer layer allows for the nearly perfect formation of GO monolayers/bilayers by scalable conventional dip-coating, and (b) incorporation into the bilayer GO structure a polymer interlayer cementing layers together and providing significant number of carbon atoms that "heal" defects and "weld" together rGO sheets during the GO reduction. A general schematic of the method is depicted in Figure 1A—E. First, we employ water-soluble, surface-active,

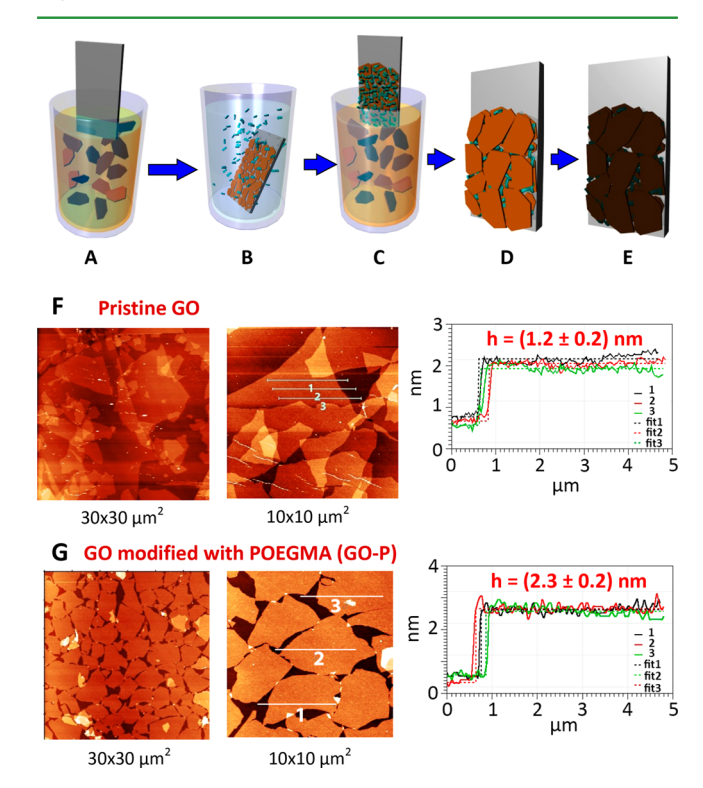


Figure 1. (A–E) Schematic representation of the method for nanomanufacturing of rGO based films. (A) Deposition of a monolayer of GO/POEGMA (GO-P) sheets enveloped with a polymer layer by dip-coating. (B) Deposition of a polymer interlayer ("linker") by adsorption. (C) Deposition of the second GO layer by dip-coating. (D) Final double layer system composed of GO. (E) Bilayer GO-P system after thermal reduction (composed of rGO-P). AFM images and corresponding cross-sectional profiles showing (F) a pristine GO layer obtained by dip-coating (vertical scale: 10 and 5 nm for 30 × 30 μ m² and 10 × 10 μ m² images, respectively) and (G) GO-P monolayer obtained by dip-coating (vertical scale: 10 and 5 nm for 30 × 30 μ m² and 10 × 10 μ m² images, respectively).

and reactive copolymer to generate a nanoscale coating evenly enveloping the GO sheets. The copolymer belongs to a class of macromolecules called molecular (or bottle) brushes that have a long polymer backbone with relatively long densely packed side chains. This coating allows the dip-coating of the GO monolayer from water-based dispersion onto the surface of nonconductive substrates. To form the bilayered rGO structure, a polymer interlayer is deposited on the GO monolayer by adsorption. Specifically, the adsorption deposition process is based on the formation of a complex between the copolymer, covering the GO sheets and the polymer linker. The linker is

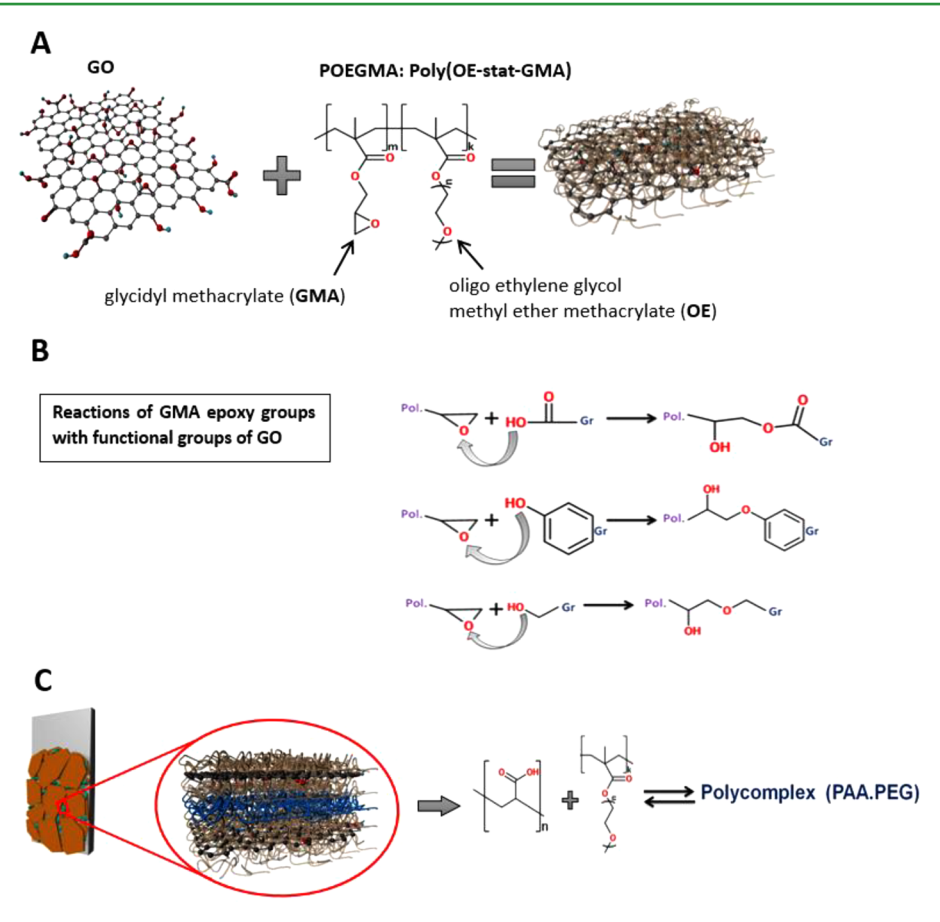


Figure 2. (A) Modification of GO sheets with POEGMA polymer. (B) Reactions of GMA epoxy groups with functional groups of GO. (C) GO-P bilayer system composed of GO/POEGMA layer, PAA linker layer (blue), and second GO/POEGMA layer.

employed to promote the formation of the second GO monolayer (by dip-coating) and provides carbon atoms for the rGO sheets' "healing" and "welding" during the GO reduction. To fabricate conductive films, the layer is reduced by high-temperature treatment to obtain rGO.

RESULTS AND DISCUSSION

Formation of GO Monolayer. The statistical copolymer (POEGMA) used for the GO modification consists of two different methacrylic monomeric units (reactive via epoxy group and hydrophobic glycidyl methacrylate [GMA] and the polar oligoethylene glycol methyl ether methacrylate [OE] responsible for solubility of the POEGMA in water) (Figure 2A). OE has oligomeric poly(ethylene glycol) [PEG] in the side moiety. We used the OE monomer with long PEG side chains (M_w of ~950 g/mol and degree of polymerization $n \approx$ 22) to obtain the copolymer. The POEGMA has a molar ratio of monomer units of 65% OE and 35% GMA, and the weight ratio between monomers is 94% OE and 6% GMA. At this ratio, where large oligomeric PEG side chains are densely decorating the copolymer linear backbone, the synthesized macromolecule is an example of a molecular brush.³⁴ During the modification of GO with POEGMA, GMA epoxy groups react with (hydroxyl, carboxyl, and epoxy) GO functional groups (Figure 2B). 35,36 The presence of multiple reactive groups along the polymer chain is needed to ensure that every macromolecule will form multiple connections with GO surface to form the thin polymer coating enveloping the sheets. It is necessary to highlight that the suspension of the GO sheets

modified with POEGMA is stable for a long time. In fact, we used the same suspension for the formation of GO layers for up to 6 months. This observation indicates that the copolymer chains anchored to the GO surface provide an effective steric stabilization of the colloidal suspension.

To determine the thickness of the individual GO sheets modified with POEGMA, we used atomic force microscopy (AFM). As indicated by the cross-sectional analysis (Figure 1F), the thickness of the pristine GO sheet was on the level of 1 nm, which is comparable to the value typically reported for the GO sheets obtained via the Hummers method. 27,37,38 However, the thickness increased more than 2-fold to ~2.5 nm (Figure 1G) upon the GO modification with copolymer. This implies that the POEGMA monolayer was indeed anchored to the GO surface. Also, the height profile of GO/POEGMA sheets (GO-P) (Figure 1G) suggested that the POEGMA chains formed even and dense coating encapsulating the sheets. We further confirmed the successful attachment of the copolymer to the GO surface with Fourier transform infrared spectroscopy (FTIR), X-ray photoelectron spectroscopy (XPS), and thermogravimetric analysis (TGA) (Supporting Information, Figures S1 and S2).

In our initial experiments with pristine (unmodified with POEGMA) GO sheets, we found that it was impossible to obtain a GO dense monolayer via dip-coating. We obtained either scarce coverage (40–50%) in the first layer or random multilayered/aggregated deposition with local wrinkles when concentration of the GO suspension was increased (Figure 1F). On the contrary, the GO-P sheets formed a dense monolayer

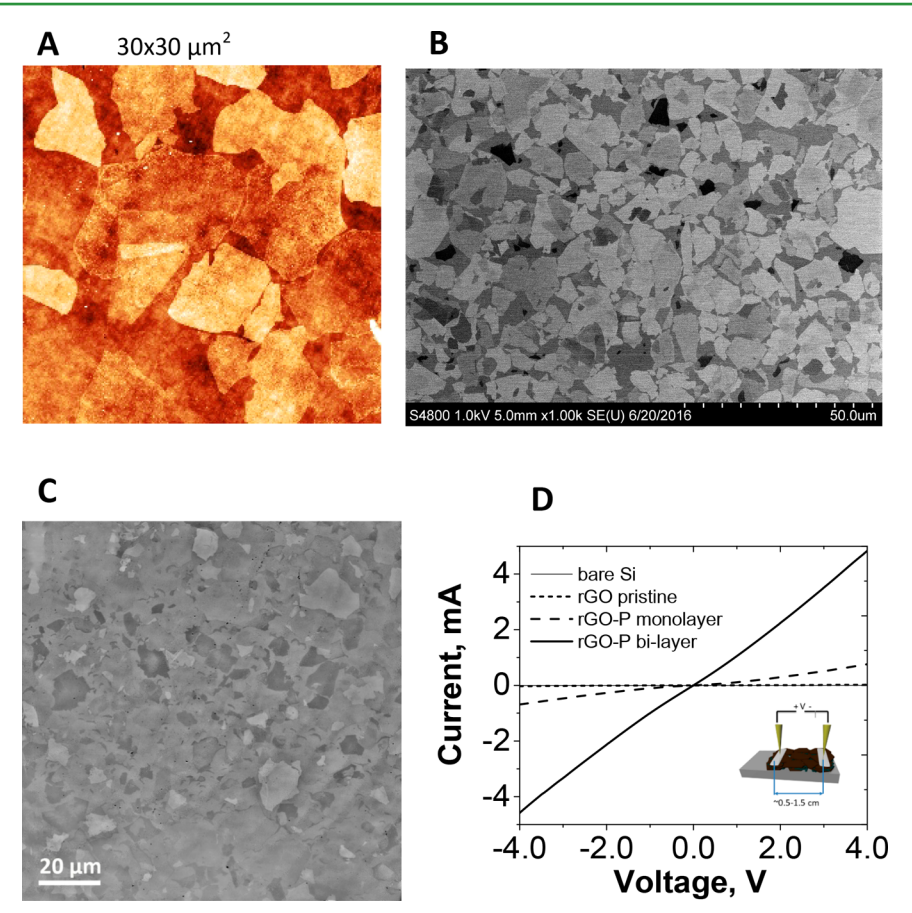


Figure 3. (A–C) Morphology of thermally reduced rGO-P monolayers deposited on undoped Si wafer. (A) AFM topography image (vertical scale: 10 nm). (B) SEM image and (C) optical image. (D) I-V curves acquired under ambient conditions for bare silicon and rGO samples. All samples were thermally reduced at 1000-1100 °C in the presence of argon gas.

(surface coverage more than 90%) as a result of the dip-coating at a quite high (300 mm/min) withdrawing speed (Figure 1G). The virtual absence of the second layer was observed by AFM as well. It is evident that the POEGMA coating sterically stabilized the GO sheets and prevented the interaction between the sheets during the deposition. At the same time, the POEGMA layer offered strong adhesion to the silicon oxide surface and the modified GO due to reaction between epoxy functional groups of GMA and silanol groups present on the surface of silicon wafer.³⁹ In fact, a dried GO-P monolayer does not delaminate from the surface in water even after an intensive 1 h ultrasonication treatment (Figure S3).

Characteristics of Reduced GO Monolayer. We examined properties of the reduced GO-P (rGO-P) monolayer obtained with the aid of POEGMA modification. For this purpose, the monolayer was deposited on an undoped (nonconductive) Si wafer. GO-P thermal reduction was conducted at 1000-1100 °C in an inert atmosphere. This process is reported to enable removal of oxygen-containing functional groups via dissociation of CO/CO₂ molecules.³⁸ The dissociation process is accompanied by formation of atomic vacancies in the carbon lattice, which are rapidly saturated with residual oxygen to form quite temperature stable carbonyl and/ or ether groups. In our model experiment with pristine GO sheets (no modification with POEGMA) XPS spectra (Figure S2C), indeed, showed significant presence of carbonyl/ether groups in the reduced GO sheets. The result also indicated that thermal reduction process applied is quite effective, since a significant amount of oxygen is removed from the sheets. The

C/O ratio (eq S2) is increased from 3 to 6 (or to about 86% of carbon content), which is comparable to the value typically reported for the thermal reduction of GO sheets at the temperatures used.³⁸ For rGO-P monolayer obtained at the same conditions from GO modified with POEGMA XPS spectra showed an increase of the C/O ratio (eq S2) from 2.7 to only 4.1 (Figure S2D). XPS results also indicate that significant amount of other than carbonyl/ether oxygen containing groups are present in the rGO-P monolayer. We associate this phenomenon with the POEGMA polymer (enveloping GO sheets) that contains a significant concentration of oxygen in its structure (Figure 2A and Figure S2B) and, therefore, changes chemical pathways of the reduction process. AFM, scanning electron microscopy (SEM), and optical microscopy (Figure 3) show that rGO-P monolayers preserved their integrity and structure. AFM cross-sectional measurements indicated that the obtained rGO-P sheets are 1.5-1.7 nm in thickness (Figure S4). This thickness is higher than the one typically observed for rGO sheets.³⁷ We attribute the higher thickness after the thermal treatment to presence of carbon/oxygen containing material incorporated in the rGO sheets, which originated during pyrolysis of POEGMA.

To assess the rearrangement of the carbon atoms in the basal plane during the thermal annealing, we used Raman spectroscopy. The Raman spectrum of the prepared GO-P monolayer displays the typical for GO materials carbon D (breathing modes of sp² rings) and G (the first-order scattering of the E_{2g} mode for sp² carbon lattice) band peaks at ~1353 and ~1595 cm⁻¹, respectively (Figure S5A,B). As a result of

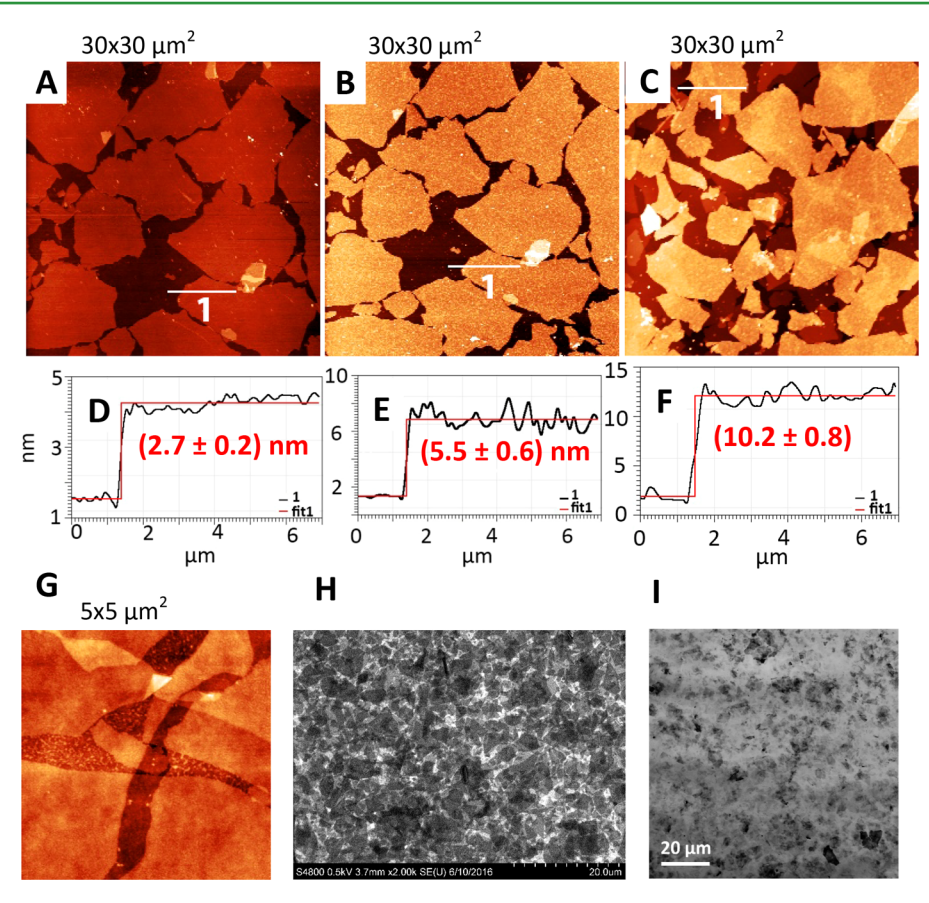


Figure 4. AFM topography images of a GO-P monolayer (A) (vertical scale: 12 nm), GO/POEGMA with adsorbed PAA layer on top (B) (vertical scale: 12 nm), and GO-P bilayer (C, C) (vertical scale: 20 and 12 nm for C0 and C0 makes C10 makes C12 nm for C12 nm for C12 nm for C13 makes C14 nm for C15 makes C15 makes C16 filling were deposited on undoped C16 filling were deposited on undoped C16 filling scale: C16 makes C17 makes C18 makes C18 makes C18 makes C18 makes C19 makes C

thermal reduction the peaks become narrower due to sp² ordering of carbon atoms. 44 The ratio of the peak intensities, D/G, is related to the degree of disorder and dimensions/ concentration of sp² ring clusters. It is frequently observed for GO materials that the ratio is increased in course of the reduction and formation of sp² strutures.^{30,43} The increase is suggested to be associated with a decrease in the average size of domains but a growth in the number of sp² domains upon reduction. 41,42 Simultaneously, the D band red-shifted by ~9 cm⁻¹, which we associate with bond disorder increase (aromatic clusters become smaller), as suggested by Ferrari et al.⁴¹ For the pristine GO reduced at the same conditions (Figure S5C,D) the D/G ratio is increased to a higher degree (from 0.96 to 1.26) and a higher red-shift was observed. Therefore, the Raman results confirm the conclusion derived from the XPS data that the reduction efficiency is lower for GO-P sheets covered with POEGMA.

To assess the electrical properties of the rGO-P monolayers, we conducted two-point I-V measurements. The distance between electrodes was between 0.5 and 0.8 cm. We report an average of three parallel samples here. The I-V curves for rGO-P monolayers (Figure 3D) revealed a nonlinear and somewhat asymmetric behavior, indicating the Schottky barrier between the contact and the film. 46 This behavior can be associated with a number of defects/traps in the material previously reported for rGO materials, such as the Poole–Frenkel effect, 47 Fowler–Nordheim tunneling, 48 and a space-charge-limited emission. 49,50 We also note that the samples prepared from pristine

GO (no prior POEGMA modification, Figure 1F) and having higher C/O ratio demonstrate much lower value of conductivity (Figure 3D). From the linear portion of the I-Vcurve (between -0.5 and +0.5 V) we estimated the sheet resistance values for rGO-P monolayers to be 23.8 k Ω /sq, and then, taking into account the thickness of individual rGO-P sheets, we found the average conductivity to be only 580 S/cm (Table S1). These results are in line with most literature reports for rGO materials. 1,2,7,13,19,20 We also carried out van der Pauw Hall effect measurements⁵¹ to extract charge carrier mobility values for our samples. The value for the rGO-P monolayer was estimated to be 65 cm² V⁻¹ s⁻¹. This value is significantly (order of magnitude) lower than the highest mobility values reported for rGO. 52,53 It is obvious that the presence of the large number of trap states caused by the defects significantly diminishes the carrier mobility. The rGO-P monolayer fabricated on quartz plate had a quite high transparency of 93% in the UV-vis region (Figure S6), which yields an optical conductivity ratio $(\sigma_{DC}/\sigma_{OP})$ on the level of 0.2.

Formation of GO Bilayer. We concluded that the electrical and optical characteristics for the rGO-P monolayers were quite encouraging for the material with such a low C/O ratio of 4.1 but definitely needed further improvement. We have hypothesized that further improvement in the conductivity will be associated with a decrease in the intersheet resistance via the addition of a second rGO-P monolayer above the first one. We had foreseen that the bilayered structure, where sheets from the top layer are placed over the sheet-to-sheet contact of the

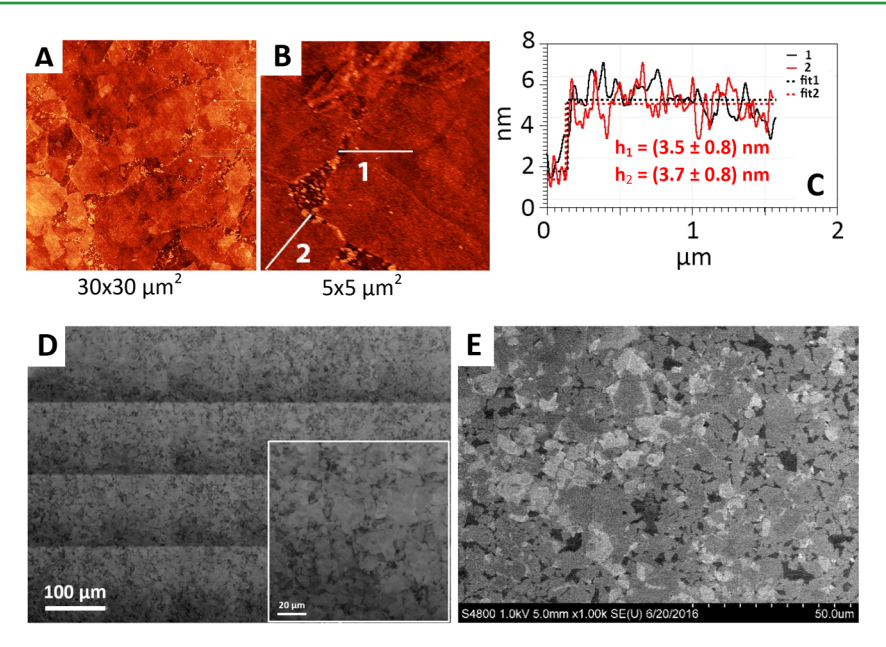


Figure 5. (A–C) AFM topographical ($30 \times 30 \ \mu\text{m}^2$ and $5 \times 5 \ \mu\text{m}^2$ images of rGO-P bilayers deposited on undoped Si wafer and AFM corresponding cross-sectional profiles. Vertical scale: 20 nm. Optical (D) and SEM (E) images of rGO-P bilayer film deposited on undoped Si wafer. Lines of the optical $700 \times 475 \ \mu\text{m}^2$ image are artifact originated from the software stitching of the consecutive optical images.

bottom layer, will decrease layer resistivity. In addition, we used a polymer linker between the sheets, poly(acrylic acid) (PAA), which during thermal reduction can serve as a carbon source for the defect "healing" 38,54,55 and "welding" of the sheets. In fact, TGA measurements showed that during heating in an inert atmosphere PAA material produced a significant amount of carbon, 15% by the polymer weight, which is significantly larger than the 5% produced during POEGMA decomposition (Figure S2E). Therefore, an external supply of carbon can saturate carbon vacancies forming as a result of $\rm CO/CO_2$ dissociation during the thermal treatment.

The PAA linker layer was adsorbed on the dip-coated GO-P monolayer (Figures 1C and 4A,B) using the approach previously employed for the L-b-L deposition of hydrogenbonded multilayers. 56,57 Namely, we utilized the complex formation between poly(ethylene glycol) side chains of POEGMA and PAA at pH values below 3. 58 AFM imaging confirmed the successful deposition of the PAA layer, as indicated by changes in morphology as well as increase in the roughness and thickness of the individual GO-P sheets (Figure 4D,E). The result of the AFM cross-section measurements indicated that a PAA layer of about 2.5-3 nm was anchored to the GO-POEGMA sheets. The employment of PAA did not require any additional modification of the GO/POEGMA material, and the same suspension of GO-P in water was used for the formation of the second GO-P monolayer. The second GO-P layer was readily deposited over the first one modified with PAA by dip-coating using the same experimental parameters as for the first layer's deposition (Figure 4C,F). The virtually uniform double-layer structure with total thickness of ~10 nm was fabricated this way (Figure 4C,F-I). It should be noted that the second GO-P layer "heals" the empty areas not covered by the first layer joining individual GO-P sheets and forming a monolithic coherent bilayer structure. It is very important that the surface was found to be virtually free of the extra third-layer presence. We found that without the PAA layer a complete second GO-P layer could not be obtained via dip-coating. We associate this phenomenon

with steric repulsion (caused by POEGMA chains) between the GO-P sheets already deposited on the surface and the sheets being deposited later.

Characteristics of Reduced GO Bilayer. The reduction of GO bilayer was conducted at the same conditions as the one for the GO monolayer. AFM imaging clearly showed that that the structure of the bilayer is preserved after the high-temperature reduction (Figure 5). It is necessary to note that residual carbon originating from the PAA (bright dots on the surface of the rGO-P sheets) is located in-between the top and bottom layers, creating a "welded" joint between them (Figure 5A,B). The sheets of the second top layer did not contain PAA. Therefore, their surface looks smooth and uniform for the part of the layer that has no direct plane contact with the first layer. We suggest that the numerous "welding" points play a dual role. First, they cement the entire structure, making it more robust and coherent. Second, they create multiple conduction routes for the electrons allowing the omission of nonconducting or poorly conducting regions, thus significantly improving the conductivity. In addition, from AFM images it appears that the border between the neighboring rGO sheets is smoothed out (Figures 4C and 5A,B). We suggest that this is a result of "welding" of the sheets by the carbon originated from PAA linker layer. From AFM cross-sectional profiles we estimated that the thickness of rGO-P bilayer is on the level of 3.5 nm. This value of the thickness was used in our estimation of the conductivity. Lower magnification SEM and optical images confirmed that a nearly perfect rGO bilayer was formed on the surface of the silicon wafer (Figure 5D,E).

The XPS results (Figure 6A,B) showed that after the thermal reduction the intensities of all the related oxygen peaks were sharply decreased. The C:O ratio of the bilayer rGO-P film was greatly improved to approximately 17:1 (or to about 94% of carbon content), and the C-C/C=C peak downshifted from 284.9 to 284.3 eV, indicating that the delocalized π conjugation was restored to a significant extent. ^{15,59} The C/O ratio is more than 2 times higher than the one determined for rGO sheets obtained from pristine GO. It is also 3.5 times higher than the

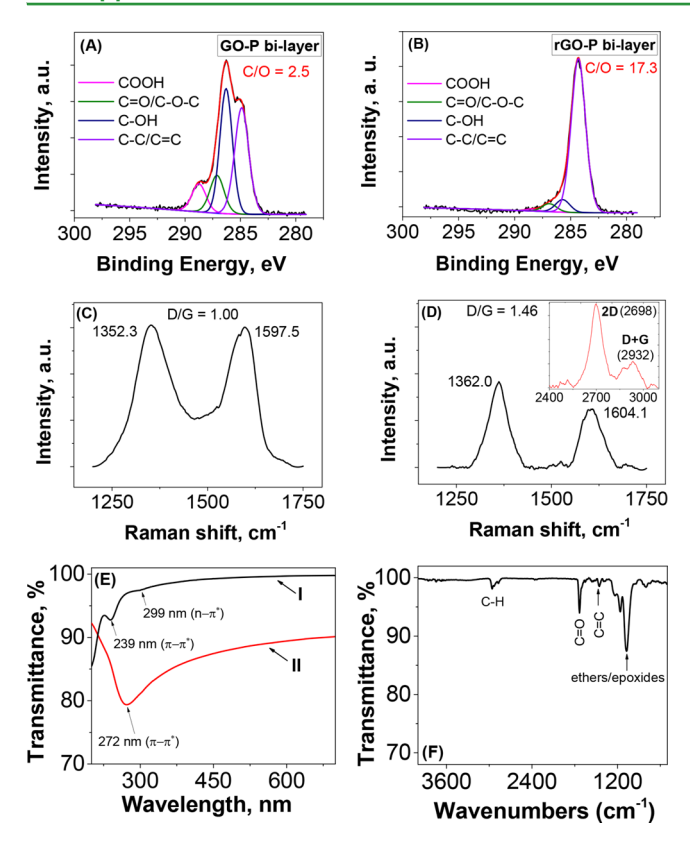


Figure 6. High-resolution C 1s spectra of GO-P bilayer film (A) and rGO-P bilayer film (B). Raman spectra of GO-P bilayer film (C) and rGO-P bilayer film (D). (E) UV-vis transmittance spectra of GP bilayer film (I) and rGO-P bilayer film (II). (F) FTIR spectrum of rGO-P bilayer film.

ratio found for rGO-P monolayer. We associate the significant increase in the C/O ratio with the carbon originating from the PAA linker layer. Raman spectroscopy confirmed efficient reduction of GO-P bilayer as well (Figure 6C,D). The D and G peaks become sharper and D/G intensity ratio significantly increased from ~1.00 to ~1.46, which indicates increase in number of the conductive sp² domains. 41,42,60 Simultaneously, a blue-shift of ~10 and ~7 cm⁻¹ was observed for the D and G bands, respectively. Moreover, a 2D band of around 2700 cm⁻¹ was readily detectable. These characteristics are indicative of the change in electron bands 41,44,45 caused by the transition from amorphous carbon to nanocrystalline graphite or sp² clustering and conjugation recovery (graphitization). 41,55

To assess the electrical properties of the rGO-P bilayers, we conducted two-point I-V measurements. The distance between electrodes was between 0.5 and 1.5 cm. We report an average of 13 independent measurements on nine different bilayer samples. We found a virtually metallic property (closeto-linear *I*–*V* curve) for the bilayer film in contrast to the rGO-P monolayer (Figure 3D). The electrical properties for all samples are listed in Table S2. The two-point transport measurements indicated an average sheet resistance of 1.170 \pm 0.487 k Ω /sq, which resulted in average conductivities of 3250 ± 2376 S/cm. We associate the relatively high standard deviation for our samples with manual handling of the each sample (e.g., positioning of the samples in dip-coater grip). We expect that the consistency of the samples can be greatly improved with more precise automatic/robotic sample handling/alignment. In this respect for the three best samples

the sheet resistance and conductivity are 0.490 \pm 0.150 k Ω /sq and $(0.7 \pm 0.26) \times 10^4$ S/cm, respectively. Our measurements indicated that to the best of our knowledge, we obtained rGO nanoscale films with the highest conductivity ever reported. It is also necessary to note that the rGO-P bilayer conductivity is fairly close to the conductivity of indium tin oxide, which is $\sim 10^4$ S/cm. 11,12 We conducted van der Pauw Hall effect measurements⁵¹ to extract charge carrier mobility values for our samples. We obtained an average value of $\sim 500 \text{ cm}^2 \text{ V}^{-1} \text{ s}^{-1}$ for the rGO bilayer, which is in good agreement with the highest mobility values reported for rGO. 52,53 Similarly, for the graphene samples in direct contact with substrates, the carrier mobilities are typically in the $\sim 10^3$ cm² V⁻¹ s⁻¹ range.⁶¹ We suggest that the relatively high value of Hall mobility observed for our samples is associated with nearest-neighbor hopping transport mechanism which can be realized for reduced graphene oxide films.^{62–64}

We prepared the rGO-P bilayers on the surface of a quartz plate to determine their optical properties. AFM imaging confirmed the formation of the rGO-P bilayer film on the quartz slide with the similar structure as that for the one fabricated on the silicon wafer (Figure S7). The sheet resistance and conductivity of the film were also comparable to the parameters of the rGO film deposited on the silicon wafer (Table S3). The UV-vis spectrum for the film is presented in Figure 6E. It is shown that the rGO bilayer has an average transparency of ~89% at 550 nm in comparison with bare quartz. It is reported⁶⁵ that unreduced GO exhibits a maximum of adsorption at 231 nm (which corresponds to the $\pi \to \pi^*$ transitions of aromatic C-C bonds) and a shoulder at ~300 nm (ascribed to the n $\rightarrow \pi^*$ transitions of C=O bonds). After reduction, the maximum red-shifts to about 272 nm (as observed in our case), which is indicative of the restored electronic conjugation within the carbon framework.⁶⁶ The calculated $\sigma_{\rm DC}/\sigma_{\rm OP}$ value for the rGO-P bilayers deposited on the quartz plate was between 2 and 4.5 (Table S3). A comparison with the data in the literature clearly indicates that our $\sigma_{\rm DC}/\sigma_{\rm OP}$ ratio is one of the highest reported for rGO We also carried out Fourier transform infrared (FTIR) measurements (Figure 6F) for the rGO-P bilayer film deposited on silicon wafer and observed that the rGO-P bilayer is >94% transparent over the range of 6667-2500 nm (4000-1500 cm⁻¹). For the significant IR spectra regions the transparency is on the level of 99%. This level of IR transparency for the rGO bilayer is similar to the transparency of graphene sheets.^{6,67} It is also important to point that conductive ITO films have very low transparency in IR spectral region.⁶⁸ Therefore, rGO-P bilayer films reported here have definite advantage in the applications requiring IR transparency of conductive coatings.

CONCLUSION

In conclusion, we have developed and demonstrated a straightforward and technology-friendly dip-coating method for the production of highly conductive (up to 10⁴ S/cm) and transparent (~90%) rGO monolayers and bilayers on nonconductive substrates. The method allows for controlling the thickness of the rGO layer with single-layer precision and achieving a high coherency and robustness of the fabricated layers. Moreover, the method of deposition is environmentally friendly and does not involve toxic organic solvents, and it can utilize conventional industrial equipment and be employed for the manufacturing of rGO-based conductive films on different substrates. Given the scalability of dip-coating deposition technology, we anticipate that the commercial manufacturing of large-scale transparent (in a broad range of wavelengths) electrodes can be straightforwardly realized with the method reported.

■ EXPERIMENTAL SECTION

Preparation of Graphene Oxide Sheets. The graphene oxide (GO) aqueous suspension was prepared using the Hummers method. 14 Natural 300-mesh graphite powder (Alfa Aesar) was Natural 300-mesh graphite powder (Alfa Aesar) was added with 2.5 g of sodium nitrate (NaNO₃) in 107 mL of 98% sulfuric acid (H₂SO₄), which was cooled to 0 °C before mixing. Then 15 g of potassium permanganate (KMnO₄) was slowly added with vigorous stirring to avoid the temperature raising above 20 °C. The mixture was heated to 35 \pm 3 °C and maintained for 30 min before adding 214 mL of water; we then waited for the temperature to raise to 98 °C and maintained at this temperature for 15 min. Finally, 850 mL of warm ultrapure water and 1-2 mL of 30% hydrogen peroxide (H₂O₂) were added sequentially to dissolve the side products of the oxidation (black particulates), during which the color of the solution turned from dark brown to bright yellow. The as-synthesized graphene oxide suspension was purified via water rinsing and ultracentrifugation (10 000 rpm for 1 h) five times to remove the electrolytes.

Synthesis of POEGMA Copolymer. Poly(glycidyl methacrylateco-oligoethylene glycol methyl ether methacrylate) (POEGMA) copolymer was synthesized by free-radical polymerization initiated by azoisobutyronitrile using glycidyl methacrylate (GMA) and oligoethylene glycol methacrylate (OEGMA, average molecular weight 950 mol/g) monomers as described elsewhere.³⁴ GMA (97%), azoisobutyronitrile (AIBN), OEGMA, and inhibitor removers (beads for removing hydroquinone and monomethyl ether hydroquinone [MEHQ] and tert-butylcatechol [BHT]) were purchased from Sigma-Aldrich. All solvents used in this study were purchased from VWR International and used as received. POEGMA was synthesized by the solution polymerization. MEHQ inhibitor remover beads were added to the GMA prior to synthesis. MEHQ and BHT inhibitor remover beads were added to the OEGMA dissolved in methyl ethyl ketone (MEK) prior to synthesis, and the suspensions were shaken for 45 min. The monomers were then filtered using 0.2 μ m syringe filters and loaded into the reaction flask with AIBN (0.01 M in monomer + MEK solution). The charged OEGMA/GMA molar ratio was 80:20, and the overall monomer concentration was 0.5 M. The solution was kept under nitrogen purge for 45 min and then immersed into a water bath preheated to 50 °C. The polymerization reaction was terminated after 1.5 h by opening the flask to the ambient atmosphere and cooling. The product of the reaction was precipitated in diethyl ether, centrifuged, and dissolved in MEK. This procedure was repeated three times to remove the unreacted monomers and initiator.

Nuclear magnetic resonance (NMR) analysis with a Bruker AVANCE-300 spectrometer, TopSpin 1.3 PL4, and Delta 5.0.4 software was used to characterize the copolymer (spectra are not shown). The OEGMA:GMA molar ratio was estimated as 68.5:31.5 and corresponds to a 94.0:6.0 mass ratio. The copolymer composition was also investigated with attenuated total reflectance Fourier transform infrared spectroscopy (spectra are not shown). A Thermo Nicolet Magna 550 Fourier transform infrared (FTIR) spectrometer with the Thermo-Spectra Tech Endurance Foundation Series Diamond ATR accessory was used, and 16 scans were averaged. An ATR correction and baseline correction were performed using Thermo Scientific OMNIC software version 8.0. Data processing and plotting were completed using Origin MicroCal 6.1. The ratio of the intensities of the peaks located at 1100 and 1727 cm⁻¹ corresponding to ether and ester bonds, respectively, was used to estimate the composition of the POEGMA:OEGMA:GMA = 63.8:36.2. Therefore, the OEG-MA:GMA molar ratio in the copolymer is approximately 66:34, as evidenced by the comparison of the NMR and FTIR measurements. The dynamic light scattering study was used to estimate the molecular weight of the POEGMA to be $M_{\rm W} \approx 2858$ kg/mol. Specifically, the Malvern Zetasizer ZS dynamic light scattering and zeta potential

(DLS-Zeta) instrument was used to measure the size of the polymer coil in methyl ethyl ketone to estimate the molecular weight. A set of monodisperse polystyrene standards with molecular weights ranging from 200 up to 3000 kDa dissolved in methyl ethyl ketone was used for calibration.

Modification of GO Sheets with POEGMA. For the modification, an aqueous suspension of GO (~1.5 mg/mL) was mixed with an aqueous solution of POEGMA (~3 mg/mL) in a mass ratio of 1:6. The mixture was vigorously shaken for 15 min and then kept at room temperature on an orbital shaker for 4 h. Next, the GO sheets were evacuated from the solution by centrifugation (Mini Spin Plus, Eppendorf) at 10 000 rpm for 5 min and rinsed six times with DI water to remove unattached macromolecules via the redispersioncentrifugation cycles. Then we centrifuged this suspension at 1000 and 500 rpm for 15 min at least two times to remove any flocculated

Formation of GO-P Monolayer. Highly polished, single-crystal, undoped nonconductive silicon wafers, cut to ~2 × 4 cm size (University Wafer: $\langle 100 \rangle$, $10\,000-20\,000$ ohm·cm, $500\,\mu\text{m}$), were used as substrates. Before deposition of the GO-P monolayer the wafers were first cleaned in an ultrasonic bath for 30 min, placed in a hot "piranha" solution (3:1 concentrated sulfuric acid 30% hydrogen peroxide) for 1 h, and then rinsed several times with high-purity DI water (18 M Ω ·cm, Nanopure). After being rinsed, the substrates were dried under a stream of ultrahigh purity nitrogen (purchased from Airgas). The GO-P mononolayer was deposited by dip-coating from 0.025 wt % GO/POEGMA suspension at a 300 mm/min withdrawal speed (Mayer Feintechnik dip coater, model D-3400).

Formation of GO-P Bilayer Film. The sample with the deposited GO-P monolayer was immersed in a 2 wt % solution of poly(acrylic acid) (PAA) with a pH of 2.5-2.8 (35 wt % water solution obtained from Sigma-Aldrich, $M_{\rm w}$ = 100 kDa) and kept there for 20 min. Then, the sample was rinsed at least three times with methanol for 15 min to remove unattached PAA from the surface and air-dried. A second layer of GO-P was deposited over the first one modified with PAA by dipcoating at a 300 mm/min withdrawal speed (Mayer Feintechnik dip coater, model D-3400).

Formation of RGO Film. The reduction of GO films on silicon substrates was done in a quartz tube using Across International STF1200 furnace. The heating program used involved blowing the wafers with Ar or N gas for 10 min, heating from room temperature to 1000 °C within 115 min (10 °C/min), maintaining that temperature for 60 min, and then cooling to room temperature within 360 min. For the formation of rGO films on quartz, the heating rate was set at 3 °C/ min. Ultrahigh-purity argon and nitrogen were purchased from Airgas.

Materials Characterization. To study the thermal decomposition of POEGMA, PAA, and the GO before and after the modification with POEGMA, TGA was performed using a Q-5000 TA Instruments and AutoTGA 2950HR V5.4A under nitrogen gas from room temperature to 700 °C using a ramp rate of 15 °C min⁻¹. A Thermo Nicolet 6700 FTIR spectrometer equipped with a transmission base plate and a "Continuum" microscope was used for the FTIR studies of the GO and GO/POEGMA materials.

Analysis of the chemical composition and the chemical states of the GO, GO-P, and rGO-P films were conducted with a Thermal Scientific K-alpha XPS using an aluminum K α radiation X-ray source (1486.7 eV). The survey scans were done by integrating the two scans between the binding energy of -10 and 1350 eV at a 1.0 eV step size and a 50 ms dwell time for each step. The high-resolution elemental spectra were collected by integrating four scans of the corresponding binding energy ranges at a 0.1 eV step size and a 50 ms dwell time. All XPS data were fit using XPSPeak 4.1 software. The background was considered to be Tougaard type, and each component peak shape was considered to be a mixture of Lorentzian and Gaussian (L/G \sim 0.3).

The morphology, microstructure, and thickness of individual GO sheets and GO/rGO films were studied with a Dimension 3100 (Veeco Digital Instruments, Inc.) atomic force microscope in the tapping mode. Silicon tips with a spring constant of 50 N m⁻¹ were used for all scans at 1 Hz. The analysis of AFM images was carried out using Gwyddion freeware version 2.45.

Optical microscopy was performed using an Olympus LEXT OLS 4000 confocal laser microscope. Scanning electron microscopy (SEM) was performed using Hitachi S-4800 with accelerating voltages of ~ 1.0 kV.

Raman spectra were recorded directly from the samples (quartz was used as a substrate) using a spectrograph (SPEX, Triplemate 1377) interfaced to a thermoelectrically cooled CCD detector (Andor Technology, Model DU420A-BV) operating at −60 °C. The spectra were excited with 514.5 nm radiation from an Innova 100 (Coherent) argon ion laser. The diameter of laser beam in the Raman experiment was ~ 1 mm. The beam covered ~ 3 mm² of the sample surface (for circular cross section of laser spot). The relatively large spot size ensured that we probe multiple graphene oxide sheets in the layers. In fact, the average area of single GO sheet is $\sim 3 \times 10^{-4}$ mm², and at 80% of coverage the number of sheets that are probed within the laser spot can be approximated as $N = 0.8 \times \frac{3}{3 \times 10^{-4}} = 8000$. The laser power was between 0.1 and 0.5 W at the sample with a total acquisition time of 100 s for each measurement. The scattered light was collected in a backscattering geometry, and the instrument was calibrated using a cyclohexane/toluene, indene, or chloroform/bromoform standard depending on the desired spectral region. Raman data and spectra were processed using Origin 2016 and freeware Spekwin32 version

To measure the conductivity of the rGO-P films, we placed a mask with rectangular cutouts made from aluminum foil and Kapton tape on the wafers and sputtered 100 nm thick gold contacts through physical vapor deposition (PVD). Current-voltage (I-V) curves were produced using an HP 4156B precision semiconductor parameter analyzer and The Micromanipulator Co., Inc. (VLSI Reliability LAB), probe station. One probe was set to provide a sweep of voltages from -4 to +4 V in 0.1 V increments and the other probe as an ammeter to monitor the current. The slope of the I-V curves correlated to R^{-1} , which was used in the same manner as with the multimeter measurements through the equation $\rho = Rhd/L$ (where R is the resistance, ρ the resistivity, L the length between contact points, h the thickness of the graphene layer(s), and d the average width of the two contact points). The sheet resistance was measured by the two-point probe technique. The average thickness h of the films found from the AFM was used in converting the resistance into conductivity. We used $\sigma = 1/\rho$ to convert the resistance measurements obtained to the values of conductivity.⁶⁹ An optical microscope at low magnification was used to precisely measure the lengths between the contacts and the width of contacts. Carrier mobility was measured using Van der Pauw Ecopia HMS-3000 Hall measurement system (see Supporting Information SI 12 for measurement details).

The transparency of the reduced double-layer film was measured using UV/vis spectroscopy (Shimadzu UV3600). We used 1/8 in. thick quartz polished plates purchased from Quartz Scientific Inc. as substrate. We used a diamond cutter to achieve the desired size of the plate: 1 cm by 3 cm slides. All quartz substrates were initially cleaned with the piranha solution according to the same procedure as that for Si wafers. The spectrum of the original cleaned plate was used as baseline in our measurements.

ASSOCIATED CONTENT

S Supporting Information

The Supporting Information is available free of charge on the ACS Publications website at DOI: 10.1021/acsami.7b16500.

SI 1: equation for conductivity ratio; SI 2: Fourier transform infrared spectroscopy (FTIR); SI 3: X-ray photon spectroscopy (XPS) and thermogravimetric analysis (TGA); SI 4: stability of GO-P monolayers; SI 5: AFM images and cross sections for rGO-P monolayers; SI 6: Raman spectra of GO-P and rGO monolayers; SI 7: electrical conductivity of rGO monolayer deposited on undoped Si wafer; SI 8: UV—vis spectra for rGO-P monolayer; SI 9: electrical

conductivity of rGO-P bilayer film deposited on undoped Si wafer; SI 10: electrical conductivity of rGO-P bilayer film deposited on quartz plate; SI 11: AFM and optical images of rGO-P bilayer film deposited on a quartz plate; SI 12: carrier mobility measurements; SI 13: references (PDF)

AUTHOR INFORMATION

Corresponding Author

*E-mail: luzinov@clemson.edu (I.L.).

ORCID ®

Nikolay Borodinov: 0000-0002-8562-5629 Vladimir Tsukruk: 0000-0001-5489-0967 Igor Luzinov: 0000-0002-1604-6519

Notes

The authors declare no competing financial interest.

ACKNOWLEDGMENTS

This work was supported by the National Science Foundation via CMMI 1538215, DMR 1505234 and EPSCoR Program OIA 1655740 awards. This work was also supported by Air Force Office of Scientific Research Award FA9550-14-1-0269. M.A. was supported by the National Science Foundation REU Grant EEC 1560070, and A.G. was supported by the National Science Foundation Graduate Fellowship. The authors also thank Kim Ivey, Mark Reymatias, and Daniel Willett for their help with the study.

REFERENCES

- (1) Ferrari, A. C.; Bonaccorso, F.; Fal'ko, V.; Novoselov, K. S.; Roche, S.; Boggild, P.; Borini, S.; Koppens, F. H. L.; Palermo, V.; Pugno, N.; Garrido, J. A.; Sordan, R.; Bianco, A.; Ballerini, L.; Prato, M.; Lidorikis, E.; Kivioja, J.; Marinelli, C.; Ryhanen, T.; Morpurgo, A.; Coleman, J. N.; Nicolosi, V.; Colombo, L.; Fert, A.; Garcia-Hernandez, M.; Bachtold, A.; Schneider, G. F.; Guinea, F.; Dekker, C.; Barbone, M.; Sun, Z. P.; Galiotis, C.; Grigorenko, A. N.; Konstantatos, G.; Kis, A.; Katsnelson, M.; Vandersypen, L.; Loiseau, A.; Morandi, V.; Neumaier, D.; Treossi, E.; Pellegrini, V.; Polini, M.; Tredicucci, A.; Williams, G. M.; Hong, B. H.; Ahn, J. H.; Kim, J. M.; Zirath, H.; van Wees, B. J.; van der Zant, H.; Occhipinti, L.; Di Matteo, A.; Kinloch, I. A.; Seyller, T.; Quesnel, E.; Feng, X. L.; Teo, K.; Rupesinghe, N.; Hakonen, P.; Neil, S. R. T.; Tannock, Q.; Lofwandera, T.; Kinaret, J. Science and Technology Roadmap for Graphene, Related Two-Dimensional Crystals, and Hybrid Systems. *Nanoscale* 2015, 7, 4598–4810.
- (2) Garg, R.; Elmas, S.; Nann, T.; Andersson, M. R. Deposition Methods of Graphene as Electrode Material for Organic Solar Cells. *Adv. Energy Mater.* **2017**, *7*, 1601393.
- (3) Novoselov, K. S.; Geim, A. K.; Morozov, S. V.; Jiang, D.; Zhang, Y.; Dubonos, S. V.; Grigorieva, I. V.; Firsov, A. A. Electric Field Effect in Atomically Thin Carbon Films. *Science* **2004**, *306*, 666–669.
- (4) Bae, S.; Kim, H.; Lee, Y.; Xu, X. F.; Park, J. S.; Zheng, Y.; Balakrishnan, J.; Lei, T.; Kim, H. R.; Song, Y. I.; Kim, Y. J.; Kim, K. S.; Ozyilmaz, B.; Ahn, J. H.; Hong, B. H.; Iijima, S. Roll-to-Roll Production of 30-in. Graphene Films for Transparent Electrodes. *Nat. Nanotechnol.* **2010**, *5*, 574–578.
- (5) Kobayashi, T.; Bando, M.; Kimura, N.; Shimizu, K.; Kadono, K.; Umezu, N.; Miyahara, K.; Hayazaki, S.; Nagai, S.; Mizuguchi, Y.; Murakami, Y.; Hobara, D. Production of a 100-m-Long High-Quality Graphene Transparent Conductive Film By Roll-to-Roll Chemical Vapor Deposition and Transfer Process. *Appl. Phys. Lett.* **2013**, *102*, 023112.
- (6) Li, X. L.; Zhang, G. Y.; Bai, X. D.; Sun, X. M.; Wang, X. R.; Wang, E.; Dai, H. J. Highly Conducting Graphene Sheets and Langmuir-Blodgett Films. *Nat. Nanotechnol.* **2008**, *3*, 538–542.

- (7) Pang, S. P.; Hernandez, Y.; Feng, X. L.; Mullen, K. Graphene as Transparent Electrode Material for Organic Electronics. *Adv. Mater.* **2011**, 23, 2779–2795.
- (8) Wu, J. B.; Becerril, H. A.; Bao, Z. N.; Liu, Z. F.; Chen, Y. S.; Peumans, P. Organic solar cells with solution-processed graphene transparent electrodes. *Appl. Phys. Lett.* **2008**, *92*, 263302.
- (9) Kymakis, E.; Stratakis, E.; Stylianakis, M. M.; Koudoumas, E.; Fotakis, C. Spin Coated Graphene Films as the Transparent Electrode in Organic Photovoltaic Devices. *Thin Solid Films* **2011**, 520, 1238–1241
- (10) Biswas, S.; Drzal, L. T. A Novel Approach to Create a Highly Ordered Monolayer Film of Graphene Nanosheets at The Liquid-Liquid Interface. *Nano Lett.* **2009**, *9*, 167–172.
- (11) Granqvist, C. G.; Hultåker, A. Transparent and Conducting ITO Films: New Developments and Applications. *Thin Solid Films* **2002**, *411*, 1–5.
- (12) Hosono, H.; Ohta, H.; Orita, M.; Ueda, K.; Hirano, M. Frontier of Transparent Conductive Oxide Thin Films. *Vacuum* **2002**, *66*, 419–425
- (13) Zheng, Q. B.; Li, Z. G.; Yang, J. H.; Kim, J. K. Graphene Oxide-Based Transparent Conductive Films. *Prog. Mater. Sci.* **2014**, *64*, 200–247
- (14) Hummers, W. S.; Offeman, R. E. Preparation of Graphitic Oxide. J. Am. Chem. Soc. 1958, 80, 1339–1339.
- (15) Stankovich, S.; Dikin, D. A.; Piner, R. D.; Kohlhaas, K. A.; Kleinhammes, A.; Jia, Y.; Wu, Y.; Nguyen, S. T.; Ruoff, R. S. Synthesis of Graphene-Based Nanosheets via Chemical Reduction of Exfoliated Graphite Oxide. *Carbon* **2007**, *45*, 1558–1565.
- (16) Layek, R. K.; Nandi, A. K. A Review on Synthesis and Properties of Polymer Functionalized Graphene. *Polymer* **2013**, *54*, 5087–5103.
- (17) Shao, J.-J.; Lv, W.; Yang, Q.-H. Self-Assembly of Graphene Oxide at Interfaces. *Adv. Mater.* **2014**, *26*, 5586–5612.
- (18) Wang, X.; Zhi, L.; Müllen, K. Transparent, Conductive Graphene Electrodes for Dye-Sensitized Solar Cells. *Nano Lett.* **2008**, *8*, 323–327.
- (19) Lopez-Naranjo, E. J.; Gonzalez-Ortiz, L. J.; Apatiga, L. M.; Rivera-Munoz, E. M.; Manzano-Ramirez, A. Transparent Electrodes: A Review of the Use of Carbon-Based Nanomaterials. *J. Nanomater.* **2016**, 2016, 1–12.
- (20) Huang, X.; Yin, Z. Y.; Wu, S. X.; Qi, X. Y.; He, Q. Y.; Zhang, Q. C.; Yan, Q. Y.; Boey, F.; Zhang, H. Graphene-Based Materials: Synthesis, Characterization, Properties, and Applications. *Small* **2011**, 7, 1876–1902.
- (21) Wu, J. B.; Agrawal, M.; Becerril, H. A.; Bao, Z. N.; Liu, Z. F.; Chen, Y. S.; Peumans, P. Organic Light-Emitting Diodes on Solution-Processed Graphene Transparent Electrodes. *ACS Nano* **2010**, *4*, 43–48.
- (22) Becerril, H. A.; Mao, J.; Liu, Z.; Stoltenberg, R. M.; Bao, Z.; Chen, Y. Evaluation of Solution-Processed Reduced Graphene Oxide Films as Transparent Conductors. *ACS Nano* **2008**, *2*, 463–470.
- (23) Lim, J.; Choi, K.; Rani, J. R.; Kim, J. S.; Lee, C.; Kim, J. H.; Jun, S. C. Terahertz, Optical, and Raman Signatures of Monolayer Graphene Behavior in Thermally Reduced Graphene Oxide Films. *J. Appl. Phys.* **2013**, *113*, 183502.
- (24) Lin, X. Y.; Jia, J. J.; Yousefi, N.; Shen, X.; Kim, J. K. Excellent Optoelectrical Properties of Graphene Oxide Thin Films Deposited on A Flexible Substrate by Langmuir-Blodgett Assembly. *J. Mater. Chem. C* **2013**, *1*, 6869–6877.
- (25) Zheng, Q.-B.; Shi, L.-F.; Yang, J.-H. Langmuir-Blodgett Assembly of Ultra-Large Graphene Oxide Films for Transparent Electrodes. *Trans. Nonferrous Met. Soc. China* **2012**, 22, 2504–2511.
- (26) Zheng, Q. B.; Ip, W. H.; Lin, X. Y.; Yousefi, N.; Yeung, K. K.; Li, Z. G.; Kim, J. K. Transparent Conductive Films Consisting of Ultra Large Graphene Sheets Produced by Langmuir-Blodgett Assembly. *ACS Nano* **2011**, *5*, 6039–6051.
- (27) Zhao, J. P.; Pei, S. F.; Ren, W. C.; Gao, L. B.; Cheng, H. M. Efficient Preparation of Large-Area Graphene Oxide Sheets for Transparent Conductive Films. *ACS Nano* **2010**, *4*, 5245–5252.

- (28) Gao, X.; Jang, J.; Nagase, S. Hydrazine and Thermal Reduction of Graphene Oxide: Reaction Mechanisms, Product Structures, and Reaction Design. J. Phys. Chem. C 2010, 114, 832–842.
- (29) Gómez-Navarro, C.; Meyer, J. C.; Sundaram, R. S.; Chuvilin, A.; Kurasch, S.; Burghard, M.; Kern, K.; Kaiser, U. Atomic Structure of Reduced Graphene Oxide. *Nano Lett.* **2010**, *10*, 1144–1148.
- (30) Mattevi, C.; Eda, G.; Agnoli, S.; Miller, S.; Mkhoyan, K. A.; Celik, O.; Mastrogiovanni, D.; Granozzi, G.; Garfunkel, E.; Chhowalla, M. Evolution of Electrical, Chemical, and Structural Properties of Transparent and Conducting Chemically Derived Graphene Thin Films. *Adv. Funct. Mater.* **2009**, *19*, 2577–2583.
- (31) Panyukov, S.; Zhulina, E. B.; Sheiko, S. S.; Randall, G. C.; Brock, J.; Rubinstein, M. Tension Amplification in Molecular Brushes in Solutions and on Substrates. *J. Phys. Chem. B* **2009**, *113*, 3750–3768.
- (32) Paturej, J.; Sheiko, S. S.; Panyukov, S.; Rubinstein, M. Molecular Structure of Bottlebrush Polymers in Melts. *Sci. Adv.* **2016**, 2, e1601478
- (33) Daniel, W. F. M.; Burdynska, J.; Vatankhah-Varnoosfaderani, M.; Matyjaszewski, K.; Paturej, J.; Rubinstein, M.; Dobrynin, A. V.; Sheiko, S. S. Solvent-Free, Supersoft and Superelastic Bottlebrush Melts and Networks. *Nat. Mater.* **2015**, *15*, 183–189.
- (34) Yadavalli, N. S.; Borodinov, N.; Choudhury, C. K.; Quinones-Ruiz, T.; Laradji, A. M.; Tu, S.; Lednev, I. K.; Kuksenok, O.; Luzinov, I.; Minko, S. Thermal Stabilization of Enzymes with Molecular Brushes. *ACS Catal.* **2017**, *7*, 8675–8684.
- (35) Roghani-Mamaqani, H.; Khezri, K. Polystyrene-Attached Graphene Nanolayers by Reversible Addition-Fragmentation Chain Transfer Polymerization: a Grafting From Epoxy Groups with Various Densities. J. Polym. Res. 2016, 23, 190.
- (36) Zdyrko, B.; Luzinov, I. Polymer Brushes by the "Grafting to". *Macromol. Rapid Commun.* **2011**, *32*, 859–869.
- (37) Kulkarni, D. D.; Kim, S.; Chyasnavichyus, M.; Hu, K.; Fedorov, A. G.; Tsukruk, V. V. Chemical Reduction of Individual Graphene Oxide Sheets as Revealed by Electrostatic Force Microscopy. *J. Am. Chem. Soc.* **2014**, *136*, 6546–6549.
- (38) Rozada, R.; Paredes, J. I.; Lopez, M. J.; Villar-Rodil, S.; Cabria, I.; Alonso, J. A.; Martinez-Alonso, A.; Tascon, J. M. D. From Graphene Oxide to Pristine Graphene: Revealing the Inner Workings of the Full Structural Restoration. *Nanoscale* **2015**, *7*, 2374–2390.
- (39) Hoy, O.; Zdyrko, B.; Lupitskyy, R.; Sheparovych, R.; Aulich, D.; Wang, J. F.; Bittrich, E.; Eichhorn, K. J.; Uhlmann, P.; Hinrichs, K.; Muller, M.; Stamm, M.; Minko, S.; Luzinov, I. Synthetic Hydrophilic Materials with Tunable Strength and a Range of Hydrophobic Interactions. *Adv. Funct. Mater.* **2010**, *20*, 2240–2247.
- (40) Mattevi, C.; Eda, G.; Agnoli, S.; Miller, S.; Mkhoyan, K. A.; Celik, O.; Mastrogiovanni, D.; Granozzi, G.; Garfunkel, E.; Chhowalla, M. Evolution of Electrical, Chemical, and Structural Properties of Transparent and Conducting Chemically Derived Graphene Thin Films. *Adv. Funct. Mater.* **2009**, *19* (16), 2577–2583.
- (41) Ferrari, A. C.; Robertson, J. Interpretation of Raman Spectra of Disordered and Amorphous Carbon. *Phys. Rev. B: Condens. Matter Mater. Phys.* **2000**, *61*, 14095–14107.
- (42) Pei, S. F.; Cheng, H. M. The Reduction of Graphene Oxide. *Carbon* **2012**, *50*, 3210–3228.
- (43) Mohan, V. B.; Jayaraman, K.; Stamm, M.; Bhattacharyya, D. Physical and Chemical Mechanisms Affecting Electrical Conductivity in Reduced Graphene Oxide Films. *Thin Solid Films* **2016**, *616*, 172–182
- (44) Ferrari, A. C. Raman Spectroscopy of Graphene And Graphite: Disorder, Electron-Phonon Coupling, Doping and Nonadiabatic Effects. *Solid State Commun.* **2007**, *143*, 47–57.
- (45) Lespade, P.; Marchand, A.; Couzi, M.; Cruege, F. Characterization of Carbon Materials with Raman Microspectrometry. *Carbon* 1984, 22, 375–385.
- (46) Di Bartolomeo, A. Graphene Schottky Diodes: an Experimental Review of the Rectifying Graphene/Semiconductor Heterojunction. *Phys. Rep.* **2016**, *606*, 1–58.
- (47) Kajen, R. S.; Chandrasekhar, N.; Pey, K. L.; Vijila, C.; Jaiswal, M.; Saravanan, S.; Ng, A. M. H.; Wong, C. P.; Loh, K. P. Charge

- Transport in Lightly Reduced Graphene Oxide: A Transport Energy Perspective. J. Appl. Phys. 2013, 113, 063710.
- (48) Pandey, S.; Biswas, C.; Ghosh, T.; Bae, J. J.; Rai, P.; Kim, G. H.; Thomas, K. J.; Lee, Y. H.; Nikolaev, P.; Arepalli, S. Transition From Direct to Fowler-Nordheim Tunneling in Chemically Reduced Graphene Oxide Film. *Nanoscale* **2014**, *6*, 3410–3417.
- (49) Li, Y. M.; Ni, X. Y.; Ding, S. J. High Performance Resistive Switching Memory Organic Films Prepared Through PPY Growing on Graphene Oxide Substrate. *J. Mater. Sci.: Mater. Electron.* **2015**, 26, 9001–9009.
- (50) Joung, D.; Chunder, A.; Zhai, L.; Khondaker, S. I. Space Charge Limited Conduction with Exponential Trap Distribution in Reduced Graphene Oxide Sheets. *Appl. Phys. Lett.* **2010**, *97*, 093105.
- (51) Li, X. S.; Cai, W. W.; Jung, I. H.; An, J. H.; Yang, D. X.; Velamakanni, A.; Piner, R.; Colombo, L.; Ruoff, R. S. Synthesis, characterization, and properties of large-area graphene films. In *Graphene and Emerging Materials for Post-CMOS Applications*; Obeng, Y., DeGendt, S., Srinivasan, P., Misra, D., Iwai, H., Karim, Z., Hess, D. W., Grebel, H., Eds.; Electrochemical Society Inc.: Pennington, NJ, 2009; Vol. 19, pp 41–52.
- (52) Feng, H. B.; Cheng, R.; Zhao, X.; Duan, X. F.; Li, J. H. A Low-Temperature Method to Produce Highly Reduced Graphene Oxide. *Nat. Commun.* **2013**, *4*, 1539.
- (53) Eigler, S.; Hu, Y. C.; Ishii, Y.; Hirsch, A. Controlled Functionalization of Graphene Oxide with Sodium Azide. *Nanoscale* **2013**, *5*, 12136–12139.
- (54) López, V.; Sundaram, R. S.; Gómez-Navarro, C.; Olea, D.; Burghard, M.; Gómez-Herrero, J.; Zamora, F.; Kern, K. Chemical Vapor Deposition Repair of Graphene Oxide: A Route to Highly-Conductive Graphene Monolayers. *Adv. Mater.* **2009**, *21*, 4683–4686.
- (55) Dai, B.; Fu, L.; Liao, L.; Liu, N.; Yan, K.; Chen, Y.; Liu, Z. High-Quality Single-Layer Graphene via Reparative Reduction of Graphene Oxide. *Nano Res.* **2011**, *4*, 434–439.
- (56) Erel-Unal, I.; Sukhishvili, S. A. Hydrogen-Bonded Multilayers of a Neutral Polymer and a Polyphenol. *Macromolecules* **2008**, *41*, 3962–3970.
- (57) Sukhishvili, S. A.; Granick, S. Layered, Erasable Polymer Multilayers Formed by Hydrogen-Bonded Sequential Self-Assembly. *Macromolecules* **2002**, *35*, 301–310.
- (58) Khutoryanskiy, V. V.; Dubolazov, A. V.; Nurkeeva, Z. S.; Mun, G. A. pH Effects in the Complex Formation and Blending of Poly(Acrylic Acid) with Poly(Ethylene Oxide). *Langmuir* **2004**, *20*, 3785–3790.
- (59) Some, S.; Kim, Y.; Yoon, Y.; Yoo, H.; Lee, S.; Park, Y.; Lee, H. High-Quality Reduced Graphene Oxide by a Dual-Function Chemical Reduction and Healing Process. *Sci. Rep.* **2013**, *3*, 5.
- (60) Furio, A.; Landi, G.; Altavilla, C.; Sofia, D.; Iannace, S.; Sorrentino, A.; Neitzert, H. C. Light Irradiation Tuning of Surface Wettability, Optical, And Electric Properties of Graphene Oxide Thin Films. *Nanotechnology* **2017**, *28*, 054003.
- (61) Farmer, D. B.; Chiu, H. Y.; Lin, Y. M.; Jenkins, K. A.; Xia, F. N.; Avouris, P. Utilization of a Buffered Dielectric to Achieve High Field-Effect Carrier Mobility in Graphene Transistors. *Nano Lett.* **2009**, *9*, 4474–4478.
- (62) Abdullah, Y.; Necmi, S.; Tülay, S.; Mehmet, K. Crossover from Nearest-Neighbor Hopping Conduction to Efros—Shklovskii Variable-Range Hopping Conduction in Hydrogenated Amorphous Silicon Films. *Jpn. J. Appl. Phys.* **2009**, *48* (11R), 111203.
- (63) Bae, J. J.; Yoon, J. H.; Jeong, S.; Moon, B. H.; Han, J. T.; Jeong, H. J.; Lee, G.-W.; Hwang, H. R.; Lee, Y. H.; Jeong, S. Y.; Lim, S. C. Sensitive photo-thermal response of graphene oxide for mid-infrared detection. *Nanoscale* **2015**, *7* (38), 15695–15700.
- (64) Bhaumik, A.; Haque, A.; Taufique, M. F. N.; Karnati, P.; Patel, R.; Nath, M.; Ghosh, K. Reduced Graphene Oxide Thin Films with Very Large Charge Carrier Mobility Using Pulsed Laser Deposition. *J. Mater. Sci. Eng.* **2017**, *6*, 364.
- (65) Paredes, J. I.; Villar-Rodil, S.; Solis-Fernandez, P.; Martinez-Alonso, A.; Tascon, J. M. D. Atomic Force and Scanning Tunneling

- Microscopy Imaging of Graphene Nanosheets Derived from Graphite Oxide. *Langmuir* **2009**, 25, 5957–5968.
- (66) Li, D.; Muller, M. B.; Gilje, S.; Kaner, R. B.; Wallace, G. G. Processable Aqueous Dispersions of Graphene Nanosheets. *Nat. Nanotechnol.* **2008**, *3*, 101–5.
- (67) De, S.; King, P. J.; Lotya, M.; O'Neill, A.; Doherty, E. M.; Hernandez, Y.; Duesberg, G. S.; Coleman, J. N. Flexible, Transparent, Conducting Films of Randomly Stacked Graphene from Surfactant-Stabilized, Oxide-Free Graphene Dispersions. *Small* **2010**, *6*, 458–464.
- (68) Taylor, R. A.; Hewakuruppu, Y.; DeJarnette, D.; Otanicar, T. P. Fabrication and Comparison of Selective, Transparent Optics for Concentrating Solar Systems. In *High and Low Concentrator Systems for Solar Energy Applications X*; Plesniak, A. P., Prescod, A. J., Eds.; SPIE-Int Soc Optical Engineering: Bellingham, WA, 2015; Vol. 9559.
- (69) Schroder, D. K. Semiconductor Material and Device Characterization; John Wiley & Sons: New York, 1998.